

METHODS FOR MODELING DAMAGE IN FINITE ELEMENT CALCULATIONS

Jeffrey W. SIMONS, *Applied Research Associates, Inc*
830 E. Evelyn Ave., Suite C, Sunnyvale, CA 94086
Email: jsimons@ara.com

Steven W. KIRKPATRICK, *Applied Research Associates, Inc*
830 E. Evelyn Ave., Suite C, Sunnyvale, CA 94086
Email: skirkpatrick@ara.com

Richard W. KLOPP, *Exponent Failure Analysis Associates*
830 E. Evelyn Ave., Suite C, Sunnyvale, CA 94086
Email: rklopp@exponent.com

Lynn SEAMAN *SRI International*
333 Ravenswood Ave, Menlo Park, CA 94025
Email: lseaman@unix.sri.com

Keywords: damage model, finite element, fracture, steel, concrete

ABSTRACT

1. OBJECTIVES

Increasingly, the objective of finite element (FE) calculations is to predict the response of a structure beyond the threshold of failure. In general, predicting the initiation of failure is not as difficult as predicting the process and final resolution of the failure.

Often the mechanisms of material failure are related to microstructural processes that occur in the materials as a result of the loading conditions. For example damage can occur by slow growth of microcracks, the sudden growth of cleavage cracks, or the development of shear bands. The response of the material is then a loss of strength that may lead to the failure of a structure. It is important to realize in cases of damage, that measured force-displacement curves including the softening response after the peak load are a structural response to the damage, and should not be considered as stress-strain curves for the material.

One approach to simulating the response of structures is to explicitly model the mechanisms of damage and failure in the material. The objective of this paper is to describe some methods for modeling material damage in finite element calculations

2. METHODS

Methods are described for modeling damage in finite element calculations for five different failure processes: (1) penetration of high strength woven fabrics, (2) dynamic cracking in concrete, (3) fatigue damage to pavements, (4) fracture of steel weldments, and (5) cleavage fracture in tank car steel. In each case the models were developed based on observations of damage mechanisms observed in careful laboratory experiments. Then equations are developed that describe the evolution of damage in the material. These

damage equations were implemented into finite element codes and used to simulate structural response.

3. RESULTS

Example simulations were performed with each of the models developed. In general, it was shown that by implementing models that describe the mechanisms of damage and failure, finite element codes can be used to analyze a wide range of structural response situations including damage and failure over a wide range of loading conditions.

METHODS FOR MODELING DAMAGE IN FINITE ELEMENT CALCULATIONS

Jeffrey W. SIMONS, *Applied Research Associates, Inc*
Steven W. KIRKPATRICK, *Applied Research Associates, Inc*
Richard W. KLOPP, *Exponent Failure Analysis Associates*
Lynn SEAMAN, *SRI International*

1. INTRODUCTION

Increasingly, the objective of finite element (FE) calculations is to predict the response of a structure beyond the threshold of failure (Holmes, et al. 1993). Structural failures usually occur as a result of localized yielding and fracture, sometimes in combination with global or local buckling. In general, predicting the initiation of failure is not as difficult as predicting the process and final resolution of the failure. For example, constitutive models that can accurately describe nonlinear material behavior in standard cases of elastic-plastic response are commonly found in finite element codes. However, predicting the progression of failure after initiation is made difficult by strongly nonlinear processes such as dramatic changes in material properties and structural geometry, or by redistribution of the loads resulting from damage.

Often the mechanisms of material failure are related to microstructural processes that occur in the materials as a result of the loading conditions. For example damage can occur by slow growth of microcracks, the sudden growth of cleavage cracks, or the development of shear bands. The response of the material is a loss of strength that may lead to the failure of a structure. It is important to realize in cases of damage that measured force-displacement curves including the softening response after the peak load are a structural response to the damage, and should not be considered as stress-strain curves for the material.

One approach to simulating the response of structures is to explicitly model the mechanisms of damage and failure in the material. The objective of this paper is to describe some methods for modeling material damage in finite element calculations.

2. METHODS

Methods are described for modeling damage in finite element calculations for five different failure processes: (1) penetration of high strength woven fabrics, (2) dynamic cracking in concrete, (3) fatigue damage to pavements, (4) fracture of steel weldments, and (5) cleavage fracture in tank car steel. In each case equations are given that describe the evolution of damage in the material. These damage equations were then implemented into finite element codes and used to simulate structural response. To perform these calculations, one of two finite element codes were used: either DYNA3D, developed by Lawrence Livermore National Laboratory [Whirley, 1993] or LS-DYNA developed by J. Hallquist [1997].

3. RESULTS

3.1 High Strength Fabrics

A finite element model for a high strength fabric (Zylon) was developed as part of a program for the Federal Aviation Administration (FAA) to mitigate the effects of uncontained engine fragments [Shockey et al., 1997]

The fabrics are produced by weaving high strength yarns. One important characteristic response of the high strength yarn is that under tension it has very little stiffness until the fibers align and straighten out. To implement a continuum treatment of this response an orthotropic constitutive model was used with a low shear modulus in planes oriented along the axial direction of the yarn.

A procedure for damage and failure was also implemented into this material model. The Zylon yarns are comprised of about 250 fibers. The damage model assumes that the fibers are elastic until they break at which point they lose all strength. Thus, the stress in the yarn is a function of the strain and the number of broken yarns,

$$\mathbf{s}_y = E(1-D)\mathbf{e}_y \quad (1)$$

where \mathbf{s}_y is axial stress in the yarn, \mathbf{e}_y is the axial strain in the yarn and D is the fraction of broken fibers. We assume that the fibers break at a uniform rate between a minimum and maximum value of strain (e.g., 0.024 and 0.052). Thus the stress rate equation is given by,

$$\dot{\mathbf{s}}_y = E(1-D)\dot{\mathbf{e}}_y - E\mathbf{e}_y \frac{\partial D}{\partial \mathbf{e}_y} \dot{\mathbf{e}}_y \quad (2)$$

Equation (2) demonstrates an important feature of the yarn response. The first term on the right is the increase in load due to stretching the unbroken fibers. The second term is the loss in load due to breaking new fibers. A drop in stress for a positive strain rate will occur the loss in stress due to fiber breakage is greater than the increase in elastic strain of the unbroken fibers.

The calculational response of this model was tested by performing simulations of single uncrimped and crimped yarn pulled axially. Figure 1 shows the finite element mesh for a short section of an uncrimped yarn. The mesh is constructed of solid elements, with eight elements in the cross section. The geometry is modeled to match photographs taken of a yarn cross section. The amount of crimp is representative of that found in yarns in a 30 x 30 pitch fabric weave.



Figure 1. Finite element mesh of a yarn segment

Figure 2 shows the stress developed in an uncrimped yarn as it is pulled, compared to a tested yarn. At a nominal strain of about 0.025 the stress levels out at 4.3 GPa and the yarn breaks at a nominal strain value of 0.032 (local strain values are higher).

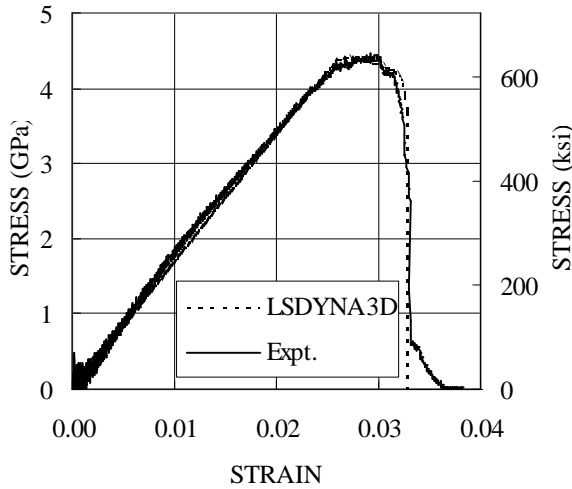


Figure 2. Calculated response of an uncrimped yarn.

To investigate the response of woven fabrics the impact of a small fragment against a patch of fabric was simulated as shown in Figure 3. Finite element simulations of the impact resistance of woven Zylon fabric were used to investigate the effect of boundary conditions and the effect of the size of the patch on ballistic performance.

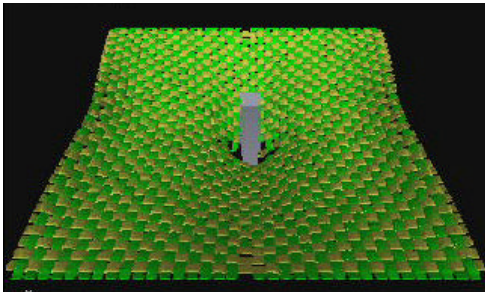


Figure 3. Simulation of fragment impact on Zylon fabric.

3.2 Dynamic Cracking in Concrete

In concrete, the physical basis for damage is the growth of cracks. A physically-based constitutive model was developed that describes growth of tensile cracks in concrete [Simons et al, 1997]. The constitutive relations are incorporated into a multiplane cracking model implemented into the finite element code DYNA2D [Whirley, 1992]. Local

stresses are introduced to account for local stress variations caused by the aggregates. Time-dependence arises from the finite propagation velocities of the microcracks

The model assumes that the total strain can be decomposed into an elastic component and a cracking component. In a local coordinate system, along an axis normal to the cracking plane we have,

$$e^t = e^e + e^c \quad (3)$$

where e^t is the total strain, e^e is the elastic strain and e^c is the cracking strain. Assuming penny-shaped cracks, the cracking strain for a set of noninteracting tensile cracks can be related to the remotely applied stress, s , as follows, [Sneddon and Lowengrub 1969]

$$e^c = \frac{16(1-\nu^2)}{3E} Na^3 s \quad s > 0 \quad (4)$$

where E is the Young's modulus and ν is the Poisson's ratio for the elastic material, N is the number of cracks per volume, and a is the crack radius.

Here, we define the compliance of the set of cracks in tension, C^c as,

$$C^c = \frac{16(1-\nu^2)}{3E} Na^3 \quad (5)$$

From Hook's law, the elastic response of the material can be expressed as,

$$e^e = \frac{s}{E} = C^e s \quad (6)$$

where C^e is the elastic compliance. We can combine Eqs. (3-6) to obtain,

$$e^t = (C^e + C^c) s \quad (7)$$

Expressing Eq. (9) in rate form, and realizing that the cracking compliance is a function of crack radius gives,

$$\dot{e}^t = (C^e + C^c) \dot{s} + \dot{C}^c s \quad (8)$$

Combining this with Eq. (7) and rearranging gives,

$$\dot{s} = (C^e + C^c)^{-1} \left(\dot{e}^t - \frac{3C^c \dot{a}}{a} s \right) \quad (9)$$

This equation reveals the mechanisms for strain softening and rate dependence in the concrete model. The second strain rate term, $(3C^c \dot{a}/a)s$, is the cracking strain rate associated with an increase in crack radii at a given stress level. Because \dot{a} is always positive, this term reduces the stress whenever the crack growth rate is non-zero. If this term is greater than the applied strain rate, \dot{e}^t , the stress rate will become negative for a positive applied strain rate, i.e., softening will occur. Thus, the mechanism for softening is the transfer of elastic strain into cracking strain.

In the model, cracking can occur on a discrete number of predetermined planes as shown in Figure 4, that may be randomly or preferentially oriented, depending on the nature and distribution of pre-existing flaws in the material.

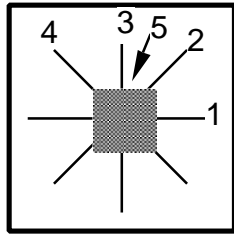


Figure 4. Crack orientations in two dimensions.

Cracks on different planes evolve independently, but their combined effect on the overall response of the material is accounted for within the framework of the compliance-based formulation. A dynamic crack growth law is given by Tsai [1973] as,

$$\frac{K_I^d}{K_I^s} = g\left(\frac{\dot{a}_I}{c_{\max}}\right) \quad (10)$$

where K_I^s and K_I^d are the static and dynamic mode I stress intensity factors, respectively, and c_{\max} is the maximum crack velocity in mode I (equal to a fraction of the Rayleigh wave velocity).

We modeled uniaxial tension tests performed by Gopalaratnam and Shah [1985]. In these experiments the concrete specimen was a notched rectangular prism 30.5 cm (12 in.) tall, 7.6 cm (3 in) wide and 1.9 cm (3/4 in) thick. The loading was applied by shear grips on either end of the specimen. The specimen was notched to predetermine the location of failure. The specimens were tested quasistatically.

The simulated load-displacement curve for the specimen loaded in uniaxial tension is shown in Figure 5 along with records from two experiments.

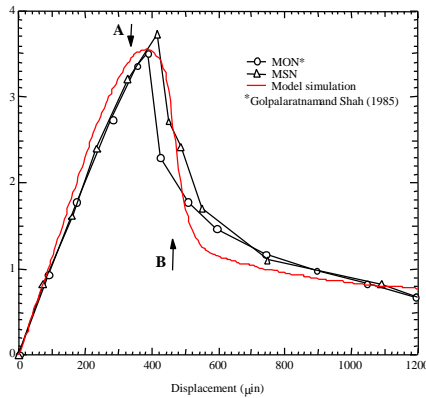


Figure 5. Simulation of notched tension test.

The applied stress reported is the applied load averaged over the notched cross section. At point A, at peak load, small cracks have nucleated throughout the specimen, above and below the material inside the notches, and cracks have started to grow from the

notches into the specimen. At point B, after the load has dropped to about 1/3 of the peak, tension cracks have developed over much of the material between the notches. This example shows how growing cracks leads to softening behavior in concrete.

3.3 Fatigue Cracking in Pavement

As part of the FHWA's truck pavement interaction (TPI) research program a finite element model was developed to estimate the fatigue cracking lifetime for pavement under traffic loads [Simons, Seaman and Kenis, 1998]. The model combines a limited number of FE simulations (spread throughout the lifetime) with a technique for extrapolating these simulations to represent the full number of loadings.

The basis for the fatigue analysis is data from tests with repeated loads in the laboratory and field. In most all cases, the data are fitted to a standard relation of the form,

$$N = \left(\frac{f}{s}\right)^n \quad (11)$$

where, N is the number of loadings to failure (or other defined level of damage), s is the maximum stress measured during each cycle, f is a critical stress and n is the exponent characterizing the resistance of the material to fatigue damage.

The model assumes that fatigue cracks grow slowly throughout the life of the pavement and uses as a basis, the Paris model which gives crack growth in a material under repeated loadings of the same amplitude:

$$\frac{dR}{dN} = B \left(\frac{K_{I0}}{K_{Ic}}\right)^n \quad (12)$$

where, B is a numerical coefficient, K_{Ic} is the fracture toughness, and K_{I0} is the maximum value of stress intensity K_I in a loading cycle. For use in FE computations, the peak stress intensity factor K_{I0} must be replaced with the stress at any point in the cycle of loading. The following form is used for incremental fatigue crack growth using only variables that are available in FE codes, .

$$dR = \frac{nBR^{n/2}}{2} \left(\frac{2}{K_{Ic}\sqrt{p}}\right)^n s^{n-1} |ds| \quad (13)$$

The absolute value around the differential stress allows crack growth whether the load is increasing or decreasing. This form integrates to give Paris law for a single cycle.

As in the model for concrete, the cracks grow with an orientation normal to the direction of maximum tensile stress. As the cracks grow, the material becomes more compliant in the direction normal to the crack faces.

An algorithm was implemented into DYNA3D to handle repeated loading. In this algorithm, (1) the fatigue crack growth for a single loading cycle is calculated, (2) the damage is extrapolated by multiplying the calculated crack growth in the cycle

by a specified number of cycles and adding that crack growth to the cumulative crack growth, and then (3) the loading cycle is repeated on the damaged pavement. Thus, the load is applied in cycles, and the damage is extrapolated between cycles.

The parameters needed for the repeated loading algorithm, including the period for a single cycle and the number of cycles for extrapolation, are included in the material properties specification. Providing the repeated loading information in the material properties specification and performing the extrapolation of damage in the material subroutines in DYNA3D minimizes the modifications to DYNA3D to perform repeated loading calculations.

The response of four-point bending tests performed at U. C. Berkeley (UCB) (Monismith, Hicks and Finn, 1991) was calculated. The loading history for the specimen was eight cycles with a loading time of 0.1 s for each cycle. Although the tests were performed at about 1.7 Hz, the calculations were performed at 10 Hz to reduce calculation time. Because the fundamental bending frequency of the undamaged beam is about 80 Hz, the response of the specimen at 10 Hz is quasi-static. For the repeated loading algorithm, the cracking damage was extrapolated by 2,500 cycles after each calculated loading cycle.

Figure 6 shows how the maximum crack growth in the beam increases with the number of cycles. For the first 2500 cycles the maximum crack growth is about 0.2 mm, and in the last 2500 cycles the cracks grow about 1.5 mm. Clearly cracks grow faster for damaged pavement.

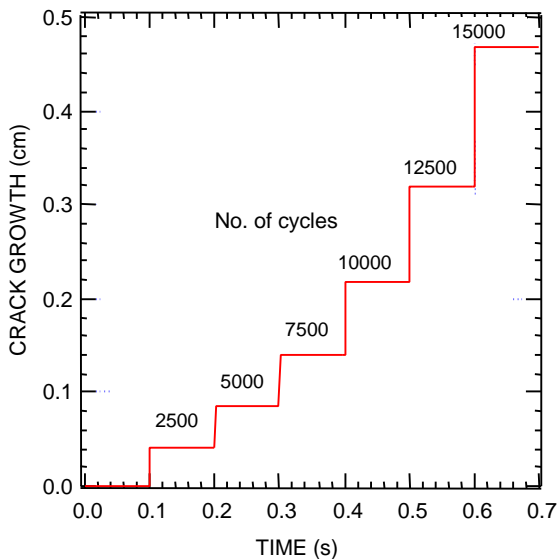


Figure 6. Maximum crack growth in bending beam.

Figure 7 shows the calculated stiffness of the specimen as a function of the number of cycles. Stiffness was calculated specimen dividing the applied load by the deflection of the center of the specimen. In the figure, we plot relative stiffness of the specimen through 15,000 cycles. The stiffness of the tests is also

shown in the figure. The agreement is fairly good, however, the calculated stiffness first drops below the experiments and then after about 10,000 cycles is slightly higher than the experiments.

From the calculations it seen that the change in beam properties due to cracking and the redistribution of stresses in the beam tests makes the response fairly complicated.

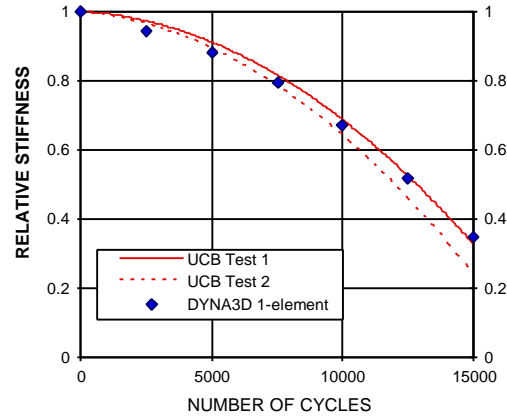


Figure 7. Loss of stiffness in bending beam.

3.4 Weld Fracture in Steel

In this example, a local fracture criterion is used to predict the fracture behavior of steel T-weldments [Giovanola and Kirkpatrick (1998)]. The purpose of the analysis was to understand the effects of weld process and experimental scale on fracture behavior. Developing the fracture model in DYNA3D required implementing a local damage model in the constitutive model and a fracture algorithm which allows discrete separation of the elements along an arbitrary fracture path within a region of the mesh. This approach allowed calculation of not only fracture initiation but also the path of fracture propagation through the structure.

T-shaped weldments were produced by welding two stiffeners normal to a slotted base plate. Each stiffener was bolted to a steel anchor, and the specimen plate was bolted to a steel die. The center of the specimen plate was loaded with strips of sheet over an area bounded by the two slots but not extending all the way to each stiffener. With this test arrangement, only the center portion of the specimen plate is significantly deformed during the experiments, while the portion supported by the die acts as a reaction frame, inducing membrane stresses in the plate. The specimens were prepared from high-strength steel. The welding process produces a heat-affected zone (HAZ) of approximately constant width, independent of the absolute weldment size. The experiment induces fractures that initiate in the plate HAZ of the weldments and then extend either through the base plate or through the stiffener.

The weldment fracture model used in this example is based on three components: (1) a material damage model formulated in terms of

plastic deformations weighted by a stress state function; (2) a geometric and strength model of the weldment, based on metallographic observations and hardness measurements; and (3) a finite element algorithm permitting independent degrees of freedom for nodes on either side of the calculated fracture path. As implemented, the fracture model is a basic form of a ductile fracture criterion (Mudry, 1985). It assumes that failure at a material location occurs when the damage within a surrounding characteristic volume (V_{MIC}) exceeds a critical value.

The damage failure criterion can be written in the form

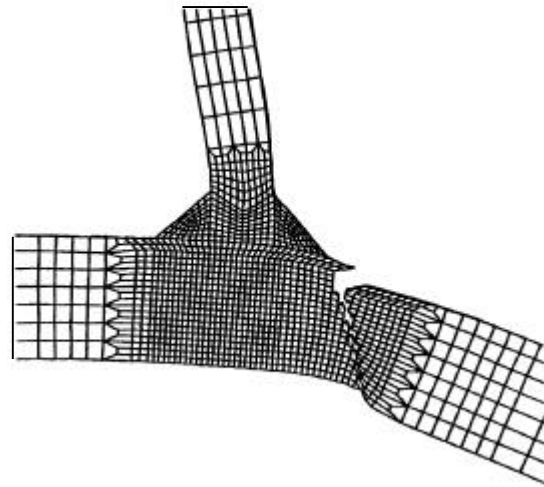
$$D = \int \frac{de_{eq}^p}{e_c(s_{mean}/s_{eq})} = 1 \quad \text{over } V_{MIC} \quad (14)$$

where D is the normalized damage parameter; de_{eq}^p is an increment in equivalent plastic strain; and $e_c(s_{mean}/s_{eq})$ is the critical failure strain as a function of the stress triaxiality, defined as the ratio of the mean stress to the equivalent stress. This critical strain function can be determined by a series of notched tensile tests with specimens of varying notch radii. V_{MIC} is a characteristic volume of the microstructural process zone.

Figure 8 shows the results of a simulation of a specimen with velocity sufficient to cause complete fracture. The crack path across the plate was faithfully reproduced in the simulation. Furthermore, the calculated deflection history was in good agreement with the experimental measurement and by lowering the initial velocity, we were able to simulate the arrest of the crack in the base plate. The good agreement between simulations and experiments partially validates the use of the fracture model for performing analyses of the weldment fracture.



(a) Experiment



(b) Calculation

Figure 8. Weld fracture.

3.5 Cleavage Fracture in Steel

A model for cleavage failure in steel was implemented in DYNA3D to investigate the validity of a set of Accident Damage Assessment Guidelines developed in the late 1970s to assist emergency response personnel in evaluating the severity of damage to pressurized tank cars involved in accidents. Laboratory fracture experiments were performed to measure the behavior of plates containing damage in the form of simulated gouges and dents. To ensure that cleavage fracture occurred, tests were performed on smooth, macroscopically unflawed TC-128B specimens at -238°F (-150°C).

The model used is the local cleavage criterion developed by Beremin [1983] and coworkers. Damage is calculated locally within the material based on the stress and strain histories and micromechanical model for the fracture processes. The prediction of cleavage fracture is different than for most ductile damage processes because there is typically large scatter in the measured cleavage fracture stress for identical tests on a single batch of material. Thus a cleavage failure criterion will ideally predict a statistical probability of fracture for a given material, geometry, and stress level, rather than a deterministic failure stress.

The microstructural processes leading to a cleavage fracture are that the material has a distribution of preexisting microcracks, typically initiated in the material from the inhomogeneities. For example, in mild steels, microcracks are produced by fracture of sulfide inclusions or grain boundary carbides. The catastrophic propagation of these cracks results in a cleavage fracture, which occurs when the stress normal to the microcrack planes reaches a critical value. This critical stress can be approximated as

$$s_c = \left[\frac{2Eg}{2(1-n)l_0} \right]^{\frac{1}{2}} \quad (15)$$

where E is Young's modulus, \underline{g} is the fracture surface energy, ν is Poisson's ratio, and l_0 is the microcrack length.

The statistical nature of the cleavage criterion is introduced by the distribution of microcrack sizes within the material. Within a given microstructural characteristic volume V_0 , the probability of finding a crack of length between l_0 and $l_0 + dl_0$ is taken as

$$P(l_0)dl_0 = \frac{a}{l_0^b} dl_0 \quad (16)$$

If we integrate the above microcrack distribution function over the range of crack lengths greater than or equal the critical crack length at a given stress level, we obtain the probability of failure as

$$P(\underline{s}) = \left(\frac{\underline{s}}{\underline{s}_u} \right)^m \quad (17)$$

where $m = 2b - 2$ and the cleavage stress, \underline{s}_u , is a material constant.

The cumulative rupture probability of the structure, combining the probabilities in each of the small representative volumes, can be approximated as,

$$P_R = 1 - \exp \left[\sum_j \frac{-V_j}{V_0} \left(\frac{\underline{s}_j}{\underline{s}_u} \right)^m \right] \quad (18)$$

Coupon tests were used to calibrate the cleavage model. First, from smooth round bar tests the true stress versus plastic strain curve for the material was obtained. This curve was then used to analyze notched round bar specimens and determine the cleavage stress. For a given value of the cleavage stress, a probability of rupture can then be determined at any load level using Eq (18).

The statistical nature of cleavage fracture can be seen by normalizing all the notched round bar failure stresses by the predicted 50% probability load level. These normalized failure stresses can then be plotted against a normalized rupture probability curve as shown in Figure 9 for the A515-70 steel. This fit is good over the full range of tests performed.

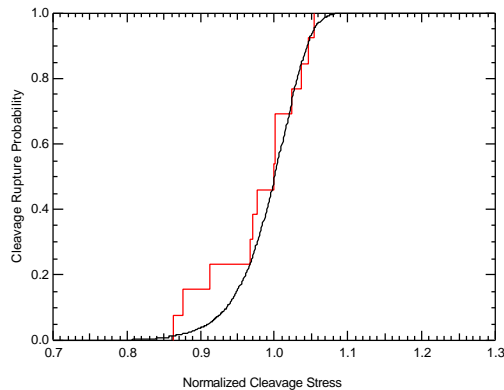


Figure 9. Normalized cleavage rupture probability.

The model was then used to predict the cleavage response of three point bend specimens as shown in Figure 10. The local fracture model calibrated using

round bar tests predicts the stress-strain and cleavage failure response of the bend specimens reasonably well. The prediction is better for more acute features such as the 1/8-inch radius gouges than for blunt features such as the 1/2-inch radius gouges and the bend specimens, but errs on the conservative side, predicting that cleavage occurs at lower stresses and strains than actually occurs in tests. Thus, the model can be applied with confidence to a wide range of tank car damage situations.

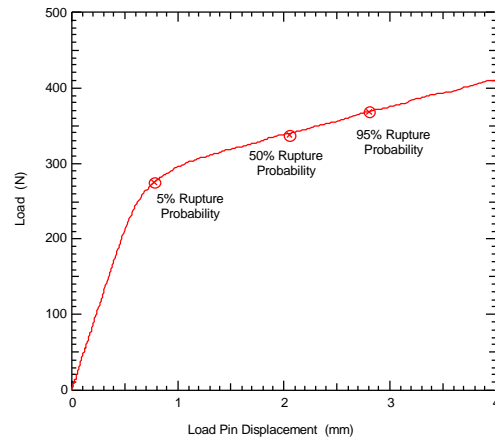


Figure 10. Probability of rupture for three-point bend tests.

4. CONCLUSIONS

Methods were described for modeling damage in finite element calculations for five different failure processes: (1) penetration of high strength woven fabrics, (2) dynamic cracking in concrete, (3) fatigue damage to pavements, (4) fracture of steel weldments, and (5) cleavage fracture in tank car steel. The example simulations showed that by modeling the mechanisms of failure, useful computational models can be implemented in finite element codes that are applicable under a wide range of loading conditions.

5. REFERENCES

Beremin, F. M., (1983), "A Local Criterion for Cleavage Fracture of a Nuclear Pressure Vessel Steel," Metallurgical Transactions A, Vol. 14A, November, 1983, pp. 2277-2287.

Giovanola, J. H., and S. W. Kirkpatrick, (1998) "Using the Local Approach to Investigate Scaling Effects in Ductile Fracture," International Journal of Fracture, Vol. 92, No. 2, pp. 101-117.

Gopalaratnam, V. S., and S. P. Shah, (1985) "Softening response of plain concrete in direct tension." *J. American Concrete Institute*, **82**(3), 310-323.

Hallquist, J. O., (1997), "LS-DYNA User's Manual", Livermore Software Technology Corporation.

Holmes, B. S., S. W. Kirkpatrick, J. W. Simons, J. H. Giovanola, and L. Seaman, (1993), "Modeling

- the Process of Failure in Structures," *Structural Crashworthiness and Failure*, T. Wierzbicki and N. Jones Eds., Elsevier Publishing Co.
- Monismith, C. L., R. G. Hicks, and F. N. Finn, (1991). "Performance-Related Testing and Measuring of Asphalt-Aggregate Interactions and Mixtures," Quarterly Technical Report, QR-UCB-003A-91-1.
- Mudry, F. (1985). Methodology and applications of local criteria for prediction of ductile tearing. In *Elastic-Plastic Fracture Mechanics*, ed. L.H. Larson. ECSC, EEC, EAEC, Brussels and Luxembourg, Belgium, pp. 263-283
- Paris, P.C., Gomez, M.P. & Anderson, W. E. (1961). A rational analytic theory of fatigue. *Trend Eng.* **13**, 9-14
- Shockey, D. A., J. H. Giovanola, J. W. Simons, D. C. Erlich, R. W. Klopp, and S. R. Skaggs, (1997),"Advanced Armor Technology: Application Potential for Engine Fragment Barriers for Commercial Aircraft", DOT/FAA/AR-97/53
- J. W. Simons, T. H. Antoun, and D. R. Curran, (1997), "A Finite Element Model for Analyzing the Dynamic Cracking Response of Concrete," Presented at 8th International Symposium on Interaction of the Effects of Munitions with Structures, McClean, Virginia, April 22-25.
- J. W. Simons, L. Seaman, and W. Kenis, (1998), "3D-FEM of Fatigue Crack Growth in Pavements", First National Symposium on 3D Finite Element Modeling for Pavement Analysis and Design, November 8-10, 1998 Charleston, West Virginia
- Tsai, Y.M., (1973), "Exact Stress Distribution, Crack Shape and Energy for a Running Penny-Shaped Crack in an Infinite Elastic Solid," *International Journal of Fracture*, **9**(2), 157-169.
- Whirley, R. G., and B. E. Engelman, (1993), "DYNA3D—A Nonlinear, Explicit, Three-Dimensional Finite Element Code for Solid and Structural Mechanics—User Manual," Report UCRL-MA-107254 Rev. 1, Lawrence Livermore National Laboratory.
- Whirley, R. G., and B. E. Engelman, (1992), "DYNA2D a Nonlinear, Explicit, Two-Dimensional Finite Element Code for Solid Mechanics, User Manual," Lawrence Livermore National Laboratory Technical Report No. UCRL-MA-110630